PASJ: Publ. Astron. Soc. Japan **60**, 37–44, 2008 February 25

Astrometry of H_2O Masers in Nearby Star-Forming Regions with VERA II SVS 13 in NGC 1333

Tomoya HIROTA,[1,2] Takeshi BUSHIMATA,[1,3] Yoon Kyung CHOI,[1,4] Mareki HONMA,[1,2] Hiroshi IMAI,[5] Kenzaburo IWADATE,[6] Takaaki JIKE,[6] Osamu KAMEYA,[2,6] Ryuichi KAMOHARA,[1] Yukitoshi KAN-YA,[7] Noriyuki KAWAGUCHI,[1,2,3] Masachika KIJIMA,[2] Hideyuki KOBAYASHI,[1,3,4,6] Seisuke KUJI,[6] Tomoharu KURAYAMA,[1] Seiji MANABE,[2,6] Takeshi MIYAJI,[1,3] Takumi NAGAYAMA,[8] Akiharu NAKAGAWA,[5] Chung Sik OH,[1,4] Toshihiro OMODAKA,[5] Tomoaki OYAMA,[1] Satoshi SAKAI,[6] Tetsuo SASAO,[9,10] Katsuhisa SATO,[6] Katsunori M. SHIBATA,[1,2,3] Yoshiaki TAMURA,[2,6] and Kazuyoshi YAMASHITA[2]

[1]*Mizusawa VERA Observatory, National Astronomical Observatory of Japan, 2-21-1 Osawa, Mitaka, Tokyo 181-8588*

[2]*Department of Astronomical Sciences, Graduate University for Advanced Studies, 2-21-1 Osawa, Mitaka, Tokyo 181-8588*

[3]*Space VLBI Project, National Astronomical Observatory of Japan, 2-21-1 Osawa, Mitaka, Tokyo 181-8588*

[4]*Department of Astronomy, Graduate School of Science, The University of Tokyo, 7-3-1 Hongo, Bunkyo-ku, Tokyo 113-0033*

[5]*Faculty of Science, Kagoshima University, 1-21-35 Korimoto, Kagoshima, Kagoshima 890-0065*

[6]*Mizusawa VERA Observatory, National Astronomical Observatory of Japan, 2-12 Hoshi-ga-oka, Mizusawa-ku, Oshu, Iwate 023-0861*

[7]*Department of Astronomy, Yonsei University, 134 Shinchong-dong, Seodaemun-gu, Seoul 120-749, Republic of Korea*

[8]*Graduate School of Science and Engineering, Kagoshima University, 1-21-35 Korimoto, Kagoshima, Kagoshima 890-0065*

[9]*Department of Space Survey and Information Technology, Ajou University, Suwon 443-749, Republic of Korea*

[10]*Korean VLBI Network, Korea Astronomy and Space Science Institute, P.O.Box 88, Yonsei University, 134 Shinchon-dong, Seodaemun-gu, Seoul 120-749, Republic of Korea*

tomoya.hirota@nao.ac.jp

(Received 2007 June 15; accepted 2007 September 10)

Abstract

We report on the results of multiepoch very long baseline interferometry (VLBI) observations with VERA (VLBI Exploration of Radio Astrometry) of the 22 GHz H_2O masers associated with the young stellar object SVS 13 in the NGC 1333 region. We carried out phase-referencing VLBI astrometry, and measured the annual parallax of the maser features in SVS 13 of 4.25 ± 0.32 mas, corresponding to a distance of 235 ± 18 pc from the Sun. Our result is consistent with a photometric distance of 220 pc, previously reported. Even though the maser features were detectable only for 6 months, the present result provides the distance to NGC 1333 with much higher accuracy than photometric methods. The absolute positions and proper motions have been derived, revealing that the H_2O masers with LSR (local standard of rest) velocities of 7–8 km s^{-1} are most likely associated with VLA 4A, which is a radio counterpart of SVS 13. It is currently difficult to attribute the observed proper motions of the maser features to either the jet or the rotating circumstellar disk associated with VLA 4A, which should be investigated through future high-resolution astrometric observations of VLA 4A and other radio sources in NGC 1333.

Key words: astrometry: — ISM: individual (NGC 1333) — ISM: jets and outflows — masers — stars: individual (SVS 13)

1. Introduction

The reflection nebula NGC 1333 is one of the nearest low-mass star-forming regions and is associated with the classical Herbig–Haro (HH) objects, HH 7–11 (7 through 11) (Herbig 1974; Strom et al. 1974). Despite the importance of NGC 1333 for studying star-formation processes and the overall structure of the larger molecular cloud complex, the distance to NGC 1333 is still quite uncertain. NGC 1333 is located in the Perseus complex of dark clouds, which forms a chain of several clouds with a size of $7^\circ \times 3^\circ$, elongated perpendicular to the Galactic plane (Černis 1990, 1993). The molecular clouds associated with NGC 1333 are located at the western edge of the chain, while the young open clusters, IC 348 and Perseus OB2, are at the eastern edge of this chain (Černis 1990, 1993).

The large-scale structure of the Perseus dark cloud complex has been studied extensively (Černis 1990, 1993; de Zeeuw et al. 1999). According to these studies, there is a gradient in distance across the complex [see figure 9 of Černis (1993)]; NGC 1333 is the nearest cloud at a distance of 220 pc (Černis 1990) and IC 348 and the Perseus OB2 association are at a distance of 318–340 pc (Černis 1993; de Zeeuw et al. 1999). Although the Hipparcos satellite provided an accurate distance to the Perseus OB2 association, based on an annual parallax measurement of 318 ± 27 pc (de Zeeuw et al. 1999), the distances to NGC 1333 and the other dark clouds have been measured only through optical photometry, with typical uncertainties of about 25% (Černis 1990, 1993). Therefore, further precise astrometry allowing an accurate annual parallax measurement is necessary to the probe of the overall structure of the chain of molecular clouds in the Perseus region.

The young stellar object (YSO) SVS 13 is located at the base of HH 7–11 in NGC 1333, and has been proposed to be a powering source of the jets and outflows in this region (Strom et al. 1976). High-resolution observations with radio interferometers at centi- and millimeter wavelengths have been conducted to investigate the complex nature of this system. Very Large Array (VLA) observations at 3.6 cm wavelength reveal a radio continuum source, VLA 4, that appears to be associated with SVS 13 (Rodríguez et al. 1997, 1999). Higher resolution VLA observations of SVS 13 at the same wavelength resolved VLA 4 into a double radio source, denoted VLA 4A and VLA 4B (Anglada et al. 2000), with a separation angle of 0.″3.

Anglada et al. (2000) reported that the position of SVS 13 coincides with the western component, VLA 4A, while the position of the millimeter source (Looney et al. 2000) is associated with the eastern component, VLA 4B. VLA 4B is suggested to have a larger amount of circumstellar material than VLA 4A, based on subsequent high-resolution VLA observations in the 7 mm band (Anglada et al. 2004).

Although HH 7–11 have been proposed to be powered by SVS 13, Rodríguez et al. (1997) argued that another radio continuum source VLA 3, located 6″ southwest of SVS 13, is a more favorable candidate for the powering source due to the alignment of VLA 3 with the HH objects. In contrast, Bachiller et al. (2000) presented the results of the interferometric CO $J = 2$–1 observations of HH 7–11, which indicate that the extremely high velocity (EHV) molecular outflow is powered by SVS 13, rather than VLA 3, which has no high-velocity CO outflow. Looney, Mundy, and Welch (2000) also suggested that VLA 3 (or millimeter source A 2 in their paper) is an unlikely candidate for the source that powers HH 7–11. Rodríguez et al. (2002) claimed that both VLA 3 and SVS 13 (VLA 4B is favorable rather than 4A) could be the powering source of HH 7–11. Despite the fact that the axes of the HH jets and molecular outflows are similar, their exciting sources could be different since there are several YSOs in a small area. In fact, it is possible that there is more than one molecular outflow because, as noted by Rodríguez et al. (2002), an inspection of figure 2 of Bachiller et al. (2000) shows that the EHV outflow is associated with VLA 4, while the standard high velocity (SHV) gas is found in the vicinity of both VLA 3 and VLA 4. Thus, the origin of the jets, molecular outflows, and HH 7–11 is still ambiguous and might be revealed through accurate proper motion measurements.

Proper motions can be accurately measured by phase-referencing VLBI observations. If one employs extragalactic radio sources as the position references, the absolute position of a target source (Beasley & Conway 1995) can be measured, making it feasible to derive its annual parallax as well as the absolute proper motion. Highly precise VLBI astrometric observations have been carried out for the Galactic CH_3OH and H_2O maser source W 3(OH) with the National Radio Astronomy Observatory (NRAO) Very Long Baseline Array (VLBA), which yielded a distance of 2.0 kpc from the Sun with uncertainties of about 2%, based on the annual parallax method (Xu et al. 2006; Hachisuka et al. 2006).

Recently, we constructed a new VLBI network in Japan, called VERA, VLBI Exploration of Radio Astrometry (Kobayashi et al. 2003), which is the first VLBI array dedicated to phase-referencing astrometry. The initial results of VERA observations have been reported (e.g., Sato et al. 2007; Honma et al. 2007; Hirota et al. 2007; Imai et al. 2007), in which the absolute proper motions and annual parallaxes were measured for Galactic H_2O maser sources at distances ranging from 178 pc for IRAS 16293−2422 (Imai et al. 2007) to 5.28 kpc for S 269 (Honma et al. 2007), demonstrating the VERA's astrometric capability.

In this paper, we present the results of the astrometry of the H_2O masers associated with SVS 13 in NGC 1333 with VERA. These observations have been conducted as one of the initial scientific projects of VERA: measurements of annual parallaxes of nearby molecular clouds (e.g., Hirota et al. 2007; Imai et al. 2007). SVS 13 is known to be one of the brightest H_2O maser sources among the known low-mass YSOs (Claussen et al. 1996; Furuya et al. 2003). In addition, there is a bright ICRF (International Celestial Reference Frame) source, J0336+3218, which is separated from SVS 13 by an angle of 1.°89 (Fey et al. 2004). The aim of the present work is to measure the distance to NGC 1333 and then to explore the powering source of the jets and outflows in this region through the maser positions and proper motions.

2. Observations

VERA observations of H_2O masers (6_{16}–5_{23}, 22235.080 MHz) associated with SVS 13 were carried out for 10 hr in each of 7 observing sessions from 2004 November to 2005 May [2004/317, 2004/355, 2005/021, 2005/052, 2005/080, 2005/113, and 2005/140; hereafter an observing session is denoted by year/(day of the year)] at intervals of about 1 month. All four stations of VERA [see figure 1 of Petrov et al. (2007)] took part in all sessions, providing a maximum baseline length of 2270 km.

Observations were made in the dual-beam mode; the H_2O masers associated with SVS 13 and a reference source, J0336+3218 (Fey et al. 2004), with a separation angle of 1.°89, were observed simultaneously. The instrumental phase difference between the two beams was measured continuously during the observation by injecting artificial noise sources into both beams at each station (Kawaguchi et al. 2000; Honma et al. 2003). The typical value of the phase drift between the two beams was 3° per hour, which was removed from the data.

Left-handed circular polarization was received and sampled with 2-bit quantization and filtered using the VERA digital filter unit (Iguchi et al. 2005). The data were recorded onto magnetic tapes at a rate of 128 Mbps, with two IF channels of 16 MHz bandwidth each for both SVS 13 and J0336+3218. J0336+3218 was detected with a peak intensity greater than 1.2 Jy beam^{-1} in all of the sessions, so it was also used for bandpass and delay calibrations. System temperatures and atmospheric attenuation were measured with the chopper-wheel method (Ulich & Haas 1976), and typical values were 100–400 K, depending on the weather conditions and the elevation angles of the observed sources. The aperture efficiencies of the antennas ranged from 45 to 52%. Correlation processing was carried out on the Mitaka FX correlator (Chikada et al. 1991) located at the National Astronomical Observatory of

Japan (NAOJ) Mitaka campus. For H_2O maser lines, the spectral resolution was set to be 15.625 kHz, corresponding to the velocity resolution of 0.21 km s^{-1}.

3. Data Reduction

Data reduction was performed using the NRAO Astronomical Image Processing System (AIPS). Amplitude and bandpass calibrations were performed for the target (SVS 13) and reference (J0336+3218) sources independently. For phase calibration, fringe fitting was done with the AIPS task FRING on the phase-reference source (J0336+3218), and the solutions were applied to the target source (SVS 13). In addition, we applied the results of the dual-beam phase calibration measurements (Kawaguchi et al. 2000). We also corrected for the approximate delay model adopted in the correlation processing (Honma et al. 2007) and for drifts of the visibility phase caused by the Earth's atmosphere based on the GPS measurements.

We first searched for H_2O maser "spots", defined as emission occurring in a single velocity channel, in fringe-rate maps with the AIPS task FRMAP. We found that the H_2O masers were detected toward two different sources in NGC 1333; one was associated with SVS 13, which was previously identified to be H_2O(A) by Haschick et al. (1980), and another was located 34″ southwest from SVS 13, corresponding to the radio continuum source VLA 2 and H_2O(B) by Haschick et al. (1980). The H_2O masers associated with VLA 2 were detected only in the first three sessions from 2004/317 to 2005/021. Because the maser spots associated with VLA 2 are 34″ southwest of the phase-tracking center, the synthesized images are significantly distorted due to the time-averaging smearing effect (Cotton 1999), making it almost impossible to maintain accuracy in astrometry. Therefore, we do not discuss the masers associated with VLA 2 in this paper.

High-resolution synthesis imaging and deconvolution (CLEAN) were carried out for the maser spots associated with SVS 13 using the AIPS task IMAGR. The image size of each map was 51.2 mas × 51.2 mas with a pixel size of 0.1 mas × 0.1 mas. The naturally weighted synthesized-beam size (FWHM) was typically 1.3 mas × 0.9 mas with a position angle of −50°. With a net integration time of 7 hr for the H_2O maser lines, the resultant rms noise levels of the phase-referenced images ranged from 0.06 Jy beam^{-1} to 0.16 Jy beam^{-1} in a single spectral channel. We regard the H_2O maser spot to be real if the signal-to-noise ratio of the peak intensity is larger than 5 times the noise level (5σ) for at least two consecutive channels, provided the positions are regarded as within range of the synthesized beam size. In order to improve the signal-to-noise ratios in the phase-referenced images, we made integrated intensity maps of the maser features, by summing the channel maps over the detected velocity range. The peak positions and intensities of the maser features were derived by fitting elliptical Gaussian brightness distributions to these integrated intensity maps using the AIPS task JMFIT. The formal uncertainties in the feature positions given by JMFIT were 0.03–0.1 mas, depending on the signal-to-noise ratios of the features, and possibly their spatial structure. The uncertainties in the peak intensities were 0.1–0.3 Jy beam^{-1} (1σ), which were approximately equal to, or slightly larger than, the rms noise levels of the phase-referenced images.

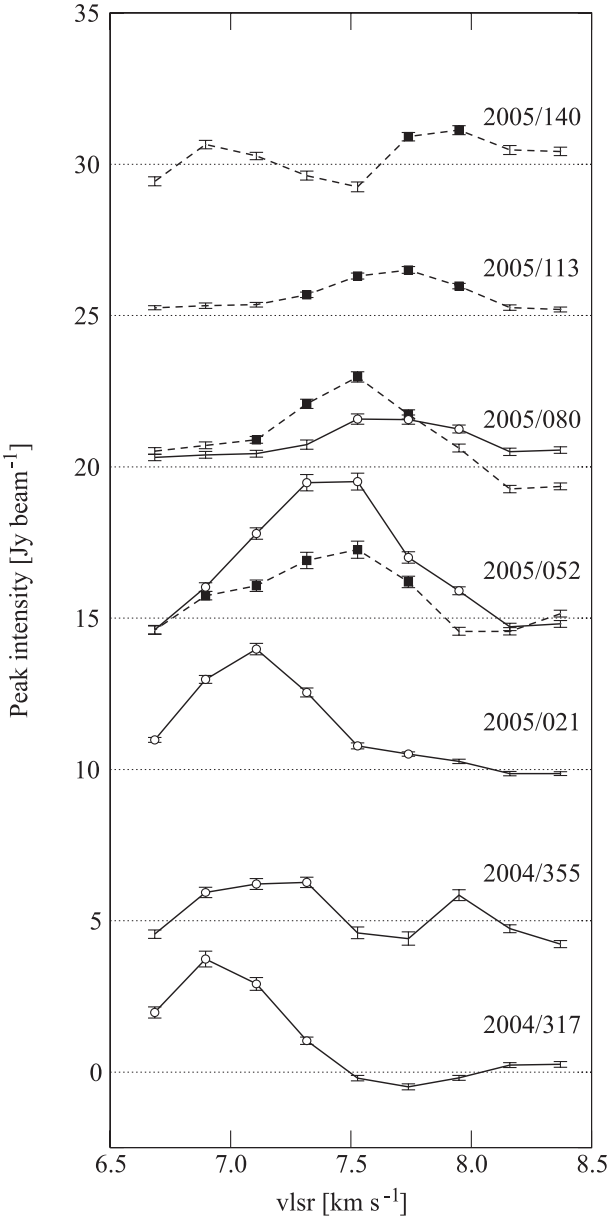

Fig. 1. Spectra of the H_2O maser features associated with SVS 13. The solid and dashed lines represent features 1 and 2, respectively. The error bars represent the fitting error (1σ) given by the AIPS task JMFIT. Maser spots with signal-to-noise ratios larger than 5 times the noise (5σ) for at least two consecutive channels are considered to be significant detections, and are plotted with open circles for feature 1 and filled squares for feature 2 (see text). For a lower signal-to-noise (non-detections) we only plot error bars. Note that negative intensities are expected due to thermal noise variations. Spectra at different epochs are offset by 5 Jy beam^{-1} steps to clarify the time variations of the spectra.

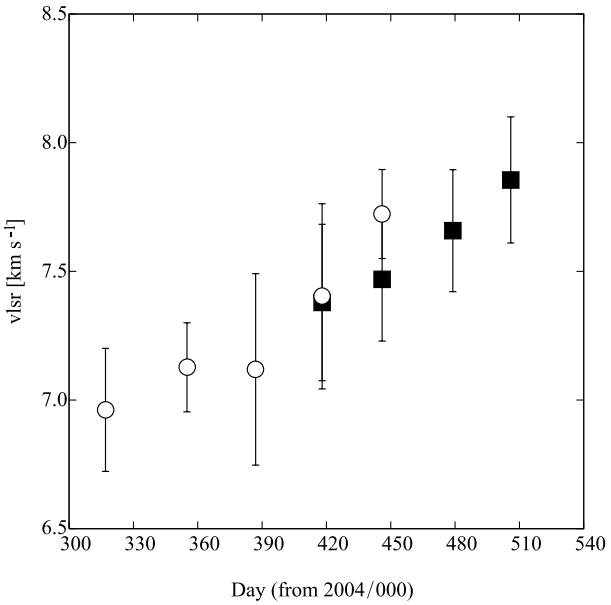

Fig. 2. Peak LSR velocities of the H_2O maser features. The open circles and filled squares represent the peak velocities for features 1 and 2, respectively, which were derived from the weighted means of the spectra shown in figure 1. Error bars indicate the standard deviation (1σ) of the velocities.

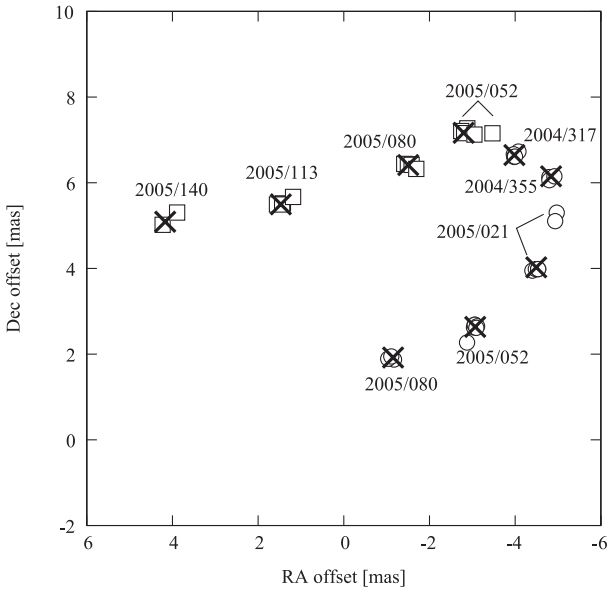

Fig. 3. Distribution of H_2O maser spots associated with SVS 13. The open circles and squares represent the positions of the maser spots belonging to features 1 and 2, respectively, while the crosses represent features that are the collections of spots integrated over contiguous spectral channels. Note that the formal errors given by the Gaussian fitting with the AIPS task JMFIT are as small as 0.1 mas or less, which cannot be shown in the figure. The positions are referred to the reference position at α(J2000.0)= $03^{\rm h}29^{\rm m}03\overset{\rm s}{.}72465$, δ(J2000.0)= $+31^\circ16'03\overset{''}{.}8015$.

4. Results

4.1. Structure of the H_2O Maser Features

Figure 1 shows the spectra of the H_2O masers associated with SVS 13, which were obtained by fitting Gaussian brightness distributions to each channel map. We detected two spatially distinct H_2O maser features at LSR velocities of 7–8 km s^{-1}, which agree well with the ambient cloud velocity (e.g., Rodríguez et al. 2002). Hereafter, we call them features 1 and 2, as explained later. We did not find other velocity components detected previously by Haschick et al. (1980), Wootten et al. (2002), and Rodríguez et al. (2002), due to the variability of the H_2O masers (e.g., Claussen et al. 1996; Furuya et al. 2003). As shown in figure 2, the peak velocity of each maser feature was found to drift systematically from 7.0 km s^{-1} to 7.9 km s^{-1} during the observing period of 6 months, at a rate of 1.7 km s^{-1} yr^{-1}. It is likely that the observed velocity drift indicates the true acceleration of the maser feature, as discussed later, although we cannot rule out the possibility of a change in strength of blended hyperfine components (Walker 1984) or in the structure of the maser feature.

Figure 3 shows the positions of the maser spots and features associated with SVS 13. Initially, we found only feature 1 in sessions 2004/317–2005/021, as seen in the spectra (figure 1). In session 2005/052, feature 2 appeared 4.5 mas north of feature 1. The two features existed at almost the same LSR velocities of about 7.5 km s^{-1} in sessions 2005/052 and 2005/080. In 2005/080, feature 2 became brighter than feature 1, which disappeared in the subsequent session 2005/113. Feature 2 remained until session 2005/140, while all of the H_2O masers associated with SVS 13 finally disappeared after the 6-month monitoring period of our observations.

We can see the internal structures of the maser features, which are collections of several maser spots, in figure 3. The dispersions of the maser spots within the features, 0.04–0.27 mas, are significantly smaller than the synthesized beam size, except for those detected in session 2005/021 in which we found two different groups of spots with a separation of 1 mas. These northern spots correspond to the weak redshifted shoulder at an LSR velocity of 7.5–7.7 km s^{-1} as can be seen in figure 1, and can be recognized as part of the elongated structure of the maser feature in the integrated intensity map. These results suggest that the peak position of the maser feature possibly affects the astrometric accuracy (e.g., Hirota et al. 2007; Imai et al. 2007), as discussed in the next section.

4.2. Astrometry of the H_2O Maser Features

As shown in figure 3, the movement of the masers significantly deviates from a simple, linear motion; as we will show, the data can be well modeled by the effect of an annual parallax. Assuming that the movement of the maser feature consists of a linear motion and the annual parallax, we derived the proper motions in right ascension, $\mu_\alpha\cos\delta$, and in declination, μ_δ, the initial positions in right ascension, α_0, and in declination, δ_0, and the annual parallax, π, for the maser feature by a least-squares analysis, as summarized in table 1 and figure 4. In the least-squares analysis, we determined the proper motions and the initial positions of two maser features independently, while the annual parallax of SVS 13 is common for both features. According to Honma et al. (2007) and Hirota et al. (2007), the precision of the derived annual

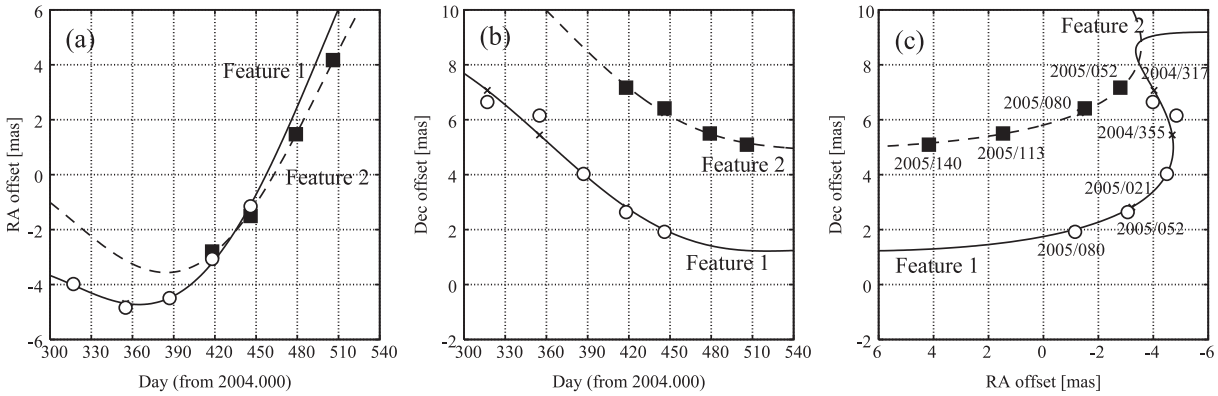

Fig. 4. Position measurements of the maser features associated with SVS 13. (a) The movement of the maser features in right ascension as a function of time. (b) The same as (a) in declination. (c) The movement of the maser features on the sky. Solid and dashed lines represent the best-fit model with the annual parallax and linear proper motion for the maser features 1 and 2, respectively. The open circles and the filled squares represent the observed positions of the maser features 1 and 2, respectively, and small crosses represent the predicted positions of the maser features. Note that the formal errors given by the Gaussian fitting with the AIPS task JMFIT are as small as 0.1 mas or less, which cannot be shown in the figure. The reference position is the same as in figure 3.

Table 1. Results of the least-squares analysis for the annual parallax and absolute proper motion measurements.

Parameter	Feature 1	Feature 2
α_0 (mas)*	−4.08(0.14)	1.17(0.36)
δ_0 (mas)*	6.14(0.31)	8.38(0.32)
$\mu_\alpha \cos\delta$ (mas yr^{-1})	17.9(0.9)	10.6(1.7)
μ_δ (mas yr^{-1})	−7.9(1.4)	−10.0(2.1)
μ (mas yr^{-1})	19.6(1.0)	14.6(1.9)
v_t (km s^{-1})	21.8(1.1)	16.3(2.1)
PA (deg)	114	133
π (mas)	4.25(0.32)	
σ_α (mas)	0.10	
σ_δ (mas)	0.29	

Numbers in parenthesis represent the estimated uncertainties. Annual parallax π is derived from the right ascension data only. σ_α and σ_δ are the rms deviations of the post-fit residuals in the right ascension and declination directions.

* The position offsets are measured with respect to the reference position.

parallax is significantly improved when we use only the data for right ascension, since this data is less affected by atmospheric modeling errors. In this manner, we find the annual parallax of the H_2O maser features associated with SVS 13 in NGC 1333 to be 4.25 ± 0.32 mas, corresponding to a distance of 235 ± 18 pc. We note that the parallax derived from the right ascension data fits the declination data quite well.

According to our astrometric results, the standard deviations of the post-fit residuals are 0.10 mas in right ascension and 0.29 mas in declination, as listed in table 1. Were we to assume distances of 300 pc and 350 pc from the Sun (similar to those of IC 348 and the Perseus OB2 association), the standard deviations in right ascension degrade to 0.19 mas and 0.26 mas, respectively. Thus, the distance to NGC 1333 is most likely 235 pc, which is consistent with the photometric distance to NGC 1333 reported by Černis (1990) of 220 pc with uncertainties of 25%, rather than the larger value of about 300 pc (e.g., Herbig & Jones 1983; de Zeeuw et al. 1999). It is the first time that the distance to NGC 1333 has been determined based on an annual parallax measurement with uncertainties of only 8%. Even though the observing period was as short as 6 months, our results provide a strong constraint on the distance to NGC 1333 with higher precision than that of the photometric method (Černis 1990).

Unfortunately, the masers associated with SVS 13 completely disappeared after the 6-month monitoring observations with VERA. We will continue long-term monitoring observations of the H_2O maser sources in NGC 1333, including SVS 13 and others such as IRAS 2 and IRAS 4 (Rodríguez et al. 2002), which may enable us to improve the accuracy of the annual parallax measurement with VERA.

Combining our new results with those of de Zeeuw et al. (1999), based on the Hipparcos measurements of the distance to the Perseus OB2 association, 318 ± 27 pc, we provide definite evidence for a distance gradient along the chain of molecular clouds in the Perseus region, as proposed by Černis (1990, 1993). Although we determine the distance to only one H_2O maser source associated with SVS 13 in NGC 1333 in this paper, we should be able to reveal the overall 3-dimensional structure of the Perseus molecular cloud complex through further VLBI astrometry of other H_2O maser sources in this region.

5. Discussions

5.1. Error Sources in Our Astrometry

The standard deviations of the post-fit residuals from the least-squares analysis, 0.10 mas in right ascension and 0.29 mas in declination, are significantly larger than the formal errors in the Gaussian fitting of the maser features, 0.03–0.1 mas, implying that some systematic errors significantly affect our astrometry. Although it is difficult to estimate the sources of systematic errors in the VLBI astrometry quantitatively (Honma et al. 2007; Hirota et al. 2007), they are mainly due to (1) the difference in the optical path lengths between the

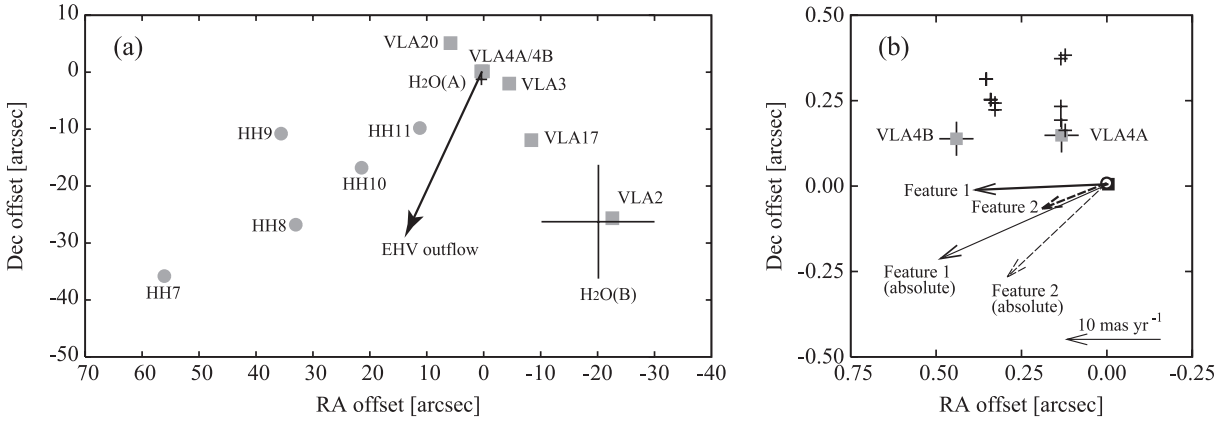

Fig. 5. Distribution of H_2O maser features associated with SVS 13 in NGC 1333. The reference position is the same as in figure 3. The H_2O maser features detected in our observations are plotted only in panel (b). (a) Grey squares indicate the positions of the radio continuum sources (Rodríguez et al. 1999; Anglada et al. 2000, 2004). Grey circles indicate the positions of HH objects (Noriega-Crespo & Garnavich 2001). Crosses represent the positions of H_2O masers denoted by H_2O(A) and H_2O(B) in Haschick et al. (1980). The size of each cross represents the error bar [1″ for H_2O(A) and 10″ for H_2O(B)]. The direction of the EHV outflow is indicated by a bold arrow (Bachiller et al. 2000). (b) Close-up view of panel (a). Grey squares with error bars (50 mas) indicate the positions of VLA 4A and 4B (Anglada et al. 2004). Small crosses represent the positions and error bars (20 mas) of the H_2O masers detected with the VLA (Rodríguez et al. 2002). An open circle and a filled square indicate the positions of the H_2O maser features 1 and 2, respectively. The absolute proper motion vectors (with respect to the Sun) for the H_2O maser features 1 and 2 are shown by thin solid and dashed arrows, respectively, while those with respect to the LSR are shown by bold solid and dashed arrows.

target and reference sources caused by the atmospheric zenith delay residual and/or (2) the variability of the structure of the maser feature for the following three reasons.

First, the optical path length error due to an atmospheric zenith delay residual of 3 cm, which is typical for VERA observations (Honma et al. 2007), would cause a relative position error of 0.3 mas, for the case of SVS 13 and J0336+3218 with a separation angle of 1.°89 at an elevation angle of 20°. This is comparable to the standard deviation of the post-fit residuals, especially in declination. Because the elevation angle of the sources was always higher than 20°, the estimated position error of 0.3 mas gives an upper limit. Nevertheless, the atmospheric zenith delay residual could contribute significantly to the error sources in our astrometry, especially in declination.

Second, the internal structures in the maser features are found to be 0.04–0.27 mas based on our channel maps of the maser spots. Sometimes, the positions of the maser spots within a feature are spread over more than 1 mas, as found in the session 2005/021. Thus structural changes might explain the 1 mas declination residual in the data point of session 2004/355 in figure 4. This data point is clearly an outlier. However, the magnitude of the possible change in the feature positions due to the variation of the internal structure of the maser spots certainly could be comparable to the dispersion of the positions of the maser spots. This effect has also been found in previous results with VERA, in particular for the H_2O maser sources associated with nearby molecular clouds (Hirota et al. 2007; Imai et al. 2007).

Third, the uncertainties in the station positions, delay model, and path length errors due to ionosphere would have negligible effects on our astrometry, according to the discussions in Honma et al. (2007). The uncertainties in the absolute position of J0336+3218 are reported to be 0.46 mas in right ascension and 0.56 mas in declination (Fey et al. 2004). These uncertainties do not affect the derived annual parallax and proper motion because they would add only a constant offset to the position of the maser feature.

In summary, we conclude that the astrometric accuracy in our observations is mainly limited by the atmospheric zenith delay error and/or the structure of the maser features.

5.2. *Origin of the H_2O Masers Associated with SVS 13*

Along with the annual parallax, we successfully measured the absolute positions and proper motions of the H_2O maser features with VERA. As shown in figure 5b, the detected maser features are likely to be physically related to VLA 4A, only 0.″2 (50 AU at the inferred distance of 235 pc) from the maser features, rather than VLA 4B or other sources. The association of the maser features in the LSR velocity of 7–8 km s^{-1} with VLA 4A is in agreement with the suggestion by Rodríguez et al. (2002). They also reported that another group of the H_2O masers at the LSR velocities ranging from -15 to -25 km s^{-1} is associated with VLA 4B, suggesting the presence of an outflow from VLA 4B (Rodríguez et al. 2002). Although the outflow activity of VLA 4B cannot be excluded by our results without any detection of the H_2O masers associated with VLA 4B, the present results show that VLA 4A is the most favorable candidate for the powering source of the observed H_2O masers.

Figure 5b and table 1 show the absolute proper motions of the maser features associated with SVS 13. Both features are moving southeast at position angles of 114° and 133°, respectively, which are apparently in agreement with the alignment of the HH objects traced by the optical emission (Noriega-Crespo & Garnavich 2001) and molecular outflows traced by the CO $J = 2$–1 line (Bachiller et al. 2000).

Although the absolute proper motions of the maser features seem to be well aligned with the jets and outflows previ-

ously reported, we must stress that the proper motions obtained with VERA do not represent the "intrinsic" proper motions of the maser features because they are measured with respect to the Sun and, hence, include the contribution of the solar motion. If we assume the solar motion relative to the LSR based on the Hipparcos satellite data, $(U_0, V_0, W_0) = (10.00, 5.25, 7.17)\,\mathrm{km\,s^{-1}}$ (Dehnen & Binney 1998), we can calculate the contribution of the solar motion to the observed absolute proper motion to be $3.7\,\mathrm{mas\,yr^{-1}}$ in right ascension and $-7.3\,\mathrm{mas\,yr^{-1}}$ in declination. Subtracting these values from the observed proper motions listed in table 1, the proper motions of the H_2O maser features with respect to the LSR in right ascension and in declination are found to be $(14.2, -0.6)\,\mathrm{mas\,yr^{-1}}$ and $(6.9, -2.7)\,\mathrm{mas\,yr^{-1}}$, for features 1 and 2, respectively, as shown in figure 5b. They are significantly different from the values based on the absolute proper motions.

Using the proper motions with respect to the LSR rather than the absolute ones, we discuss the possible origin of the H_2O masers associated with SVS 13. First, we rule out the possibility that Galactic rotation might account for the observed proper motions, because the contribution of Galactic rotation would be only $(-0.65, 0.49)\,\mathrm{mas\,yr^{-1}}$, which is estimated by assuming R_0 of 8.0 kpc (Reid 1993) and Θ_0 of $236\,\mathrm{km\,s^{-1}}$ (Reid & Brunthaler 2004).

One of the most plausible explanations is that the proper motions of the maser features are due to the jet from VLA 4A. In fact, VLA 4A is proposed to be a powering source of the HH jets and molecular outflows, as mentioned above (e.g., Bachiller et al. 2000; Noriega-Crespo & Garnavich 2001). If VLA 4A is at rest with respect to the LSR, the proper motions of the H_2O masers with respect to the LSR, $15.8\,\mathrm{km\,s^{-1}}$ ($14.2\,\mathrm{mas\,yr^{-1}}$) and $8.3\,\mathrm{km\,s^{-1}}$ ($7.4\,\mathrm{mas\,yr^{-1}}$) for features 1 and 2, respectively, represent the motions relative to VLA 4A. These observed transverse velocities are consistent with those of the jets and outflows previously observed in this region (Wootten et al. 2002). However, the directions of the proper motions are not parallel to the jets from VLA 4A (e.g., Bachiller et al. 2000; Noriega-Crespo & Garnavich 2001; Wootten et al. 2002). In addition, positions of the maser features are not exactly aligned with the HH objects and molecular outflows from VLA 4A. However, VLA 4A, itself, might hava a proper motion with respect to the LSR, which could account for the apparent discrepancy found in the geometry of VLA 4A and jets traced by the H_2O masers.

It is worth considering whether the observed proper motion is due to a rotating circumstellar disk of VLA 4A. According to Anglada et al. (2004), VLA 4B, a companion of the close binary system including VLA 4A, has a circumstellar disk with the radius and mass of < 30 AU and $0.06\,M_\odot$, respectively, while the mass of the circumstellar disk of VLA 4A is at least smaller than one fifth of VLA 4B's mass. Note, however, that we detected a signature of acceleration of the maser features, as shown in figure 2, which might be indicative of rotating disk (e.g., Miyoshi et al. 1995). If we simply assume an edge-on disk with a rotation velocity, v_{rot}, of $12\,\mathrm{km\,s^{-1}}$, which equals to the mean proper motion of the maser features, the radius of the disk, r_{d}, can be derived from the relationship $r_{\mathrm{d}} = v_{\mathrm{rot}}^2/A$ to be 18 AU, where A is the drift rate of the radial velocity of the maser features, $1.7\,\mathrm{km\,s^{-1}\,yr^{-1}}$. The inferred radius of the disk is in agreement with that of VLA 4B (< 30 AU: Anglada et al. 2004), but it is slightly smaller than the separation from VLA 4A, $\sim$50 AU. As a result, the enclosed mass within the radius of 18 AU is estimated to be $3M_\odot$. This value gives a lower limit of the mass, because we simply assume the inclination axis of the disk to be 0°. The mass of the envelope associated with SVS 13 is derived to be of the order of $1M_\odot$ based on the interferometric millimeter wave observations of dust continuum emission (e.g., Looney et al. 2000). In addition, the luminosity of SVS 13 is as low as $\sim 22L_\odot$ (Jennings et al. 1987), suggesting that it should be a low-mass YSO. Although these results agree well with the mass of $3M_\odot$, estimated from the circumstellar disk model, the position of the disk (the maser feature) and the YSO (radio continuum source) is inconsistent with the edge-on disk model.

The results of our astrometry of the maser features are still puzzling because the positions and proper motions of the maser features with respect to VLA 4A do not fully satisfy the requirements for either a jet or a rotating circumstellar disk associated with VLA 4A. One of the reasons for this discrepancy arises from the lack of the absolute proper motion measurements of VLA 4A and other possible candidates for the powering source of the masers. The proper motion vectors could be changed significantly by subtracting the absolute proper motion vector of VLA 4A, making us reconsider all of the possibilities discussed above. Other possibilities, such as an orbital motion of the binary system consisting of VLA 4A and VLA 4B (e.g., Anglada et al. 2000, 2004; Rodríguez et al. 2002), could be tested if we measure the proper motions of VLA 4A and VLA 4B. Further high-precision astrometry of the maser features together with the possible candidates for their powering sources (i.e., VLA 4A and other radio continuum sources in NGC1333) is essential to solving this problem (e.g., Rodríguez et al. 2005).

6. Summary

We present the results of multiepoch VLBI astrometric observations of the 22 GHz H_2O masers associated with SVS 13 in the NGC 1333 region with VERA. The principal results of this paper are summarized as follows:

1. We have determined the annual parallax of the H_2O masers associated with SVS 13 to be 4.25 ± 0.32 mas, corresponding to a distance of 235 ± 18 pc from the Sun. Although the inferred distance of 235 pc is consistent with the photometric distance of 220 pc, estimated by Černis (1990), our results provide the distance to NGC 1333 with much higher accuracy than the photometric method.

2. The standard deviations of the post-fit residuals for the annual parallax and proper-motion measurements are 0.10 mas in right ascension and 0.29 mas in declination. The astrometric error sources in our observations are discussed, and they are attributed to the difference in the optical path lengths between the target and reference sources caused by the atmospheric zenith delay errors and/or to the variability of the structures of the maser features.

3. The absolute positions and proper motions of the H_2O maser features at the LSR velocities of 7–8 $\mathrm{km\,s^{-1}}$ are derived, revealing that they are most likely to be associated with the

radio continuum source VLA 4A, based on the observation that the projected distances of the maser features are only 50 AU from VLA 4A.

4. We considered the possible origin of the observed proper motions of the maser features, and found it difficult to explain the positions and the proper motions of the maser features in terms of either the jet or the rotating circumstellar disk associated with VLA 4A, solely based on the present results. Further highly precise astrometric observations of the maser features and radio continuum sources, including VLA 4A, would be necessary to the probe of the complex nature found in the HH 7–11 regions in NGC 1333.

We thank the referee, Dr. Guillem Anglada, for valuable suggestions and Dr. Mark J. Reid for his critical reading of our revised manuscript, which substantially improved the paper. We are grateful to the staff of all the VERA stations for their assistance in observations. T. H. is financially supported by Grants-in-Aid from the Ministry of Education, Culture, Sports, Science and Technology (13640242 and 16540224).

References

Anglada, G., Rodríguez, L. F., Osorio, M., Torrelles, J. M., Estalella, R., Beltrán, M. T., & Ho, P. T. P. 2004, ApJ, 605, L137
Anglada, G., Rodríguez, L. F., & Torrelles, J. M. 2000, ApJ, 542, L123
Bachiller, R., Gueth, F., Guilloteau, S., Tafalla, M., & Dutrey, A. 2000, A&A, 362, L33
Beasley, A. J., & Conway, J. E. 1995, ASP Conf. Ser., 82, 327
Černis, K. 1990, Ap&SS, 166, 315
Černis, K. 1993, Baltic Astron., 2, 214
Chikada, Y., et al. 1991, in Frontiers of VLBI, ed. H. Hirabayashi, M. Inoue, & H. Kobayashi (Tokyo: Universal Academy Press), 79
Claussen, M. J., Wilking, B. A., Benson, P. J., Wootten, A., Myers, P. C., & Terebey, S. 1996, ApJS, 106, 111
Cotton, W. D. 1999, ASP Conf. Ser., 180, 357
Dehnen, W., & Binney, J. J. 1998, MNRAS, 298, 387
de Zeeuw, P. T., Hoogerwerf, R., de Bruijne, J. H. J., Brown, A. G. A., & Blaauw, A. 1999, AJ, 117, 354
Fey, A. L., et al. 2004, AJ, 127, 3587
Furuya, R. S., Kitamura, Y., Wootten, A., Claussen, M. J., & Kawabe, R. 2003, ApJS, 144, 71
Hachisuka, K., et al. 2006, ApJ, 645, 337
Haschick, A. D., Moran, J. M., Rodriguez, L. F., Burke, B. F., Greenfield, P., & Garcia-Barreto, J. A. 1980, ApJ, 237, 26
Herbig, G. H. 1974, Lick Obs. Bull., 658
Herbig, G. H., & Jones, B. F. 1983, AJ, 88, 1040
Hirota, T., et al. 2007, PASJ, 59, 897
Honma, M., et al. 2003, PASJ, 55, L57
Honma, M., et al. 2007, PASJ, 59, 889
Iguchi, S., Kurayama, T., Kawaguchi, N., & Kawakami, K. 2005, PASJ, 57, 259
Imai, H., et al. 2007, PASJ, 59, 1107
Jennings, R. E., Cameron, D. H. M., Cudlip, W., & Hirst, C. J. 1987, MNRAS, 226, 461
Kawaguchi, N., Sasao, T., & Manabe, S. 2000, Proc. SPIE, 4015, 544
Kobayashi, H., et al. 2003, ASP Conf. Ser., 306, 367
Looney, L. W., Mundy, L. G., & Welch, W. J. 2000, ApJ, 529, 477
Miyoshi, M., Moran, J., Herrnstein, J., Greenhill, L., Nakai, N., Diamond, P., & Inoue, M. 1995, Nature, 373, 127
Noriega-Crespo, A., & Garnavich, P. M. 2001, AJ, 122, 3317
Petrov, L., Hirota, T., Honma, M., Shibata, K. M., Jike, T., & Kobayashi, H. 2007, AJ, 133, 2487
Reid, M. J. 1993, ARA&A, 31, 345
Reid, M. J., & Brunthaler, A. 2004, ApJ, 616, 872
Rodríguez, L. F., Anglada, G., & Curiel, S. 1997, ApJ, 480, L125
Rodríguez, L. F., Anglada, G., & Curiel, S. 1999, ApJS, 125, 427
Rodríguez, L. F., Anglada, G., Torrelles, J. M., Mendoza-Torres, J. E., Haschick, A. D., & Ho, P. T. P. 2002, A&A, 389, 572
Rodríguez, L. F., Poveda, A., Lizano, S., & Allen, C. 2005, ApJ, 627, L65
Sato, M., et al. 2007, PASJ, 59, 743
Strom, S. E., Grasdalen, G. L., & Strom, K. M. 1974, ApJ, 191, 111
Strom, S. E., Vrba, F. J., & Strom, K. M. 1976, AJ, 81, 314
Ulich, B. L., & Haas, R. W. 1976, ApJS, 30, 247
Walker, R. C. 1984, ApJ, 280, 618
Wootten, A., Claussen, M., Marvel, K., & Wilking, B. 2002, IAU Symp., 206, 100
Xu, Y., Reid, M. J., Zheng, X. W., & Menten, K. M. 2006, Science, 311, 54